Exploring the mechanism of the hydroboration of alkenes by amine–boranes catalysed by [Rh(xantphos)]+†

Heather C. Johnson,[a] Rebecca Torry-Harris,[a] Laura Ortega,[b] Robin Theron,[c] J. Scott McIndoe[c] and Andrew S. Weller*[a]

The [Rh(xantphos)]+ fragment acts as an effective catalyst for the hydroboration of the alkene TBE (*tert*-butyl ethene) using the amine–borane $H_3B \cdot NMe_3$ at low (0.5 mol%) catalyst loadings to give the linear product. Investigations into the mechanism using the initial rate method and labelling studies show that reductive elimination of the linear hydroboration product is likely the rate-limiting step at the early stages of catalysis, and that alkene and borane activation (insertion into a Rh–H bond and B–H oxidative addition) are reversible. The resting state of the system has also been probed using electrospray ionization mass spectrometry (ESI-MS) using the pressurised sample infusion (PSI) technique. This system is not as effective for hydroboration of other alkenes such as 1-hexene, or using phosphine borane $H_3B \cdot PCy_3$, with decomposition or P–B bond cleavage occurring respectively.

Introduction

Hydroboration, the addition of a B–H bond across an unsaturated C–C bond, is a versatile methodology that affords organoboranes, from which subsequent functionalisation leads to products of use in organic synthesis.[1–4] Non-metal catalysed hydroboration generally yields the anti-Markovnikov product, whereas transition metal catalysts enable control over the regioselectivity of hydroboration. Such selectivity (*i.e.* linear *versus* branched products) has been shown to vary with different catalysts, alkenes and even reaction conditions.[5–8] Historically metal-catalysed hydroborations have used three-coordinate boron substrates such as catechol (HBCat) or pinacol borane.[2,3] By contrast four-coordinate amine–boranes (prototypically $H_3B \cdot NMe_3$) have traditionally been used in uncatalysed hydroboration where N–B cleavage is proposed to afford a reactive trivalent BH_3 molecule,[9]

although iodine-induced hydroboration is proposed to operate *via* an intermediate that retains the B–N bond.[10] Amine–boranes have, instead, received much recent attention due to their potential as hydrogen storage systems and as precursors to oligomeric or polymeric B–N materials *via* dehydro-coupling;[11] and we,[12,13] alongside others,[9,11] have been exploring the role of the metal catalyst in these processes. Recognising that B–H oxidative cleavage from a bound sigma complex to form a metal boryl hydride (Scheme 1a) is closely related to the same mode of activation of a B–H bond at a metal in hydroboration (Scheme 1b), we reported in 2011

[a] Department of Chemistry, University of Oxford, Mansfield Road, Oxford, OX1 3TA, UK. E-mail: andrew.weller@chem.ox.ac.uk
[b] Visiting Student from Departamento de Química Inorgánica, Instituto de Investigaciones Químicas (IIQ), Universidad de Sevilla, Consejo Superior de Investigaciones Científicas, Avda. Américo Vespucio 49, 41092 Sevilla, Spain
[c] Department of Chemistry, University of Victoria, P.O. Box 3065, Victoria, BC V8W 3V6, Canada

† Electronic supplementary information (ESI) available: X-ray crystallographic data collection and refinement details. Crystallographic data have been deposited with the Cambridge Crystallographic Data Center (CCDC), CCDC 1001382 (**3**) and 1001383 (**8**). For ESI and crystallographic data in CIF or other electronic format see DOI: 10.1039/c4cy00597j

Scheme 1 Rh-catalysed hydroboration using amine–borane (a) and catechol borane (b); hydroboration of TBE using $H_3B \cdot NMe_3$, (c).

3486 | *Catal. Sci. Technol.*, 2014, **4**, 3486–3494

This journal is © The Royal Society of Chemistry 2014

that the addition of the alkene *tert*-butylethene (TBE) to the sigma amine–borane complex $[Rh(P^iBu_2{}^tBu)_2(\eta^2\text{-}H_3B\cdot NMe_3)]$ $[BAr^F_4]$ resulted in the formation of the linear hydroboration product $[Rh(P^iBu_2{}^tBu)_2(\eta^2\text{-}H_2B(CH_2CH_2{}^tBu)\cdot NMe_3)][BAr^F_4]^{14}$ $[Ar^F = 3,5\text{-}(CF_3)_2C_6H_4]$. The precursor complex $[Rh(P^iBu_2{}^tBu)_2]$ $[BAr^F_4]$ also slowly (94 h, 5 mol%) catalysed this process to form free $H_2B(CH_2CH_2{}^tBu)\cdot NMe_3$ (I), Scheme 1c.
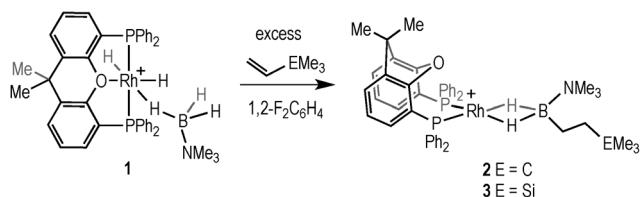
Kinetic experiments allowed for a mechanism to be proposed in which the hydroborated product inhibited catalytic turnover and reductive elimination of the product was also suggested to be slow.[15] Independently, in 2012, a similar methodology using N-heterocyclic carbene–boranes and chiral Rh-based catalysts was reported for intramolecular hydroborations of alkenes.[16] Very recently we briefly communicated that by using a $[Rh(\kappa^2{}_{P,P}\text{-xantphos})]^+$ based catalyst,[17] TBE can be hydroborated to give **I**. In the absence of this alkene, dehydrogenative homocoupling of the borane occurs (see Scheme 4), a process suggested to occur *via* the B–H activated intermediate that is no longer intercepted by coordination of alkene.[18] We now report in detail on this hydroboration, including kinetic data that support a proposed mechanism, as well as assessing the scope of this catalyst with regard to other alkenes and phosphine–boranes.

Results and discussion

Preliminary stoichiometric and catalytic studies

Addition of excess TBE to the Rh(III) sigma–borane complex $[Rh(\kappa^3{}_{P,O,P}\text{-xantphos})(H)_2(\eta^1\text{-}H_3B\cdot NMe_3)][BAr^F_4]$ **1** resulted in the rapid formation (less than 5 minutes) of the Rh(I) complex $[Rh(\kappa^2{}_{P,P}\text{-xantphos})(\eta^2\text{-}H_2B(CH_2CH_2{}^tBu)\cdot NMe_3)][BAr^F_4]$ (**2**) as the sole metal-containing product (Scheme 2), presumably by initial hydrogenation of one equivalent of alkene to form a Rh(I) species, followed by hydroboration of another equivalent. The solid-state structure and NMR spectroscopic data for **2** have previously been communicated.[18] In a similar manner, addition of trimethylvinyl silane to **1** gives the equivalent complex **3**, $[Rh(\kappa^2{}_{P,P}\text{-xantphos})(\eta^2\text{-}H_2B(CH_2CH_2SiMe_3)\cdot NMe_3)]$ $[BAr^F_4]$, in which $H_2B(CH_2CH_2SiMe_3)\cdot NMe_3$ (**II**) is bound to the metal centre.

Complex **3** was characterised by NMR spectroscopy, ESI-MS (electrospray ionisation mass spectrometry) and microanalysis, which together show similar analytical data to **2** and closely related $[Rh(P^iBu_2{}^tBu)_2(\eta^2\text{-}H_2B(CH_2CH_2{}^tBu)\cdot NMe_3)]$ $[BAr^F_4]$.[14] The alkyl borane binds to the metal centre through two sigma Rh–H–B interactions, evident by single [11]B quadrupolar-broadened signal at δ −6.54 in the ^{1}H NMR
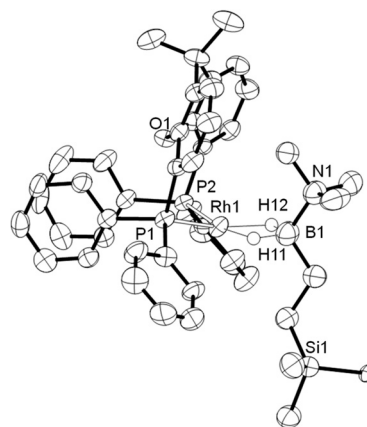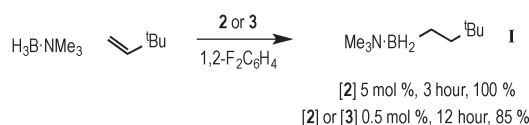

Fig. 1 Solid-state structure of the cationic portion of **3**. Displacement ellipsoids are drawn at the 50% probability level. $[BAr^F_4]^-$ anion and all carbon-bound H atoms are omitted for clarity. Only the major component of the disordered NMe_3 and $SiMe_3$ groups are shown. Selected bond lengths (Å) and angles (°): Rh1–P1, 2.2398(18); Rh1–P2, 2.2670(17); Rh1–O1, 3.2342(73); Rh1–B1, 2.179(7); B1–N1, 1.603(4); P1–Rh1–P2, 98.23(6).

spectrum of relative integral 2H, which collapses to an overlapping doublet of doublets (virtual triplet) on decoupling to [11]B [$J(RhH) = 36$ Hz, $J(P_{trans}H) = 36$ Hz]. Two, relative integral 2H, multiplets were observed at δ 1.17 and δ 0.78 for the CH_2 groups, indicating that the anti-Markovnikov (*i.e.* linear) product of hydroboration is bound to the metal centre. A ^{29}Si-^{1}H HMBC NMR experiment showed a correlation between silicon [$\delta(^{29}Si)$ 2.1] and the alkyl protons at δ 1.17, assigning these to those α to Si. The xantphos methyl groups are observed as two separate environments (δ 1.73 and δ 1.67). In the ^{11}B NMR spectrum a broad resonance is observed at δ 37, typical for η^2-coordination of an amine–borane to a Rh(I) centre,[19,20] which has shifted 45.7 ppm downfield from that in **1** (δ −8.7).[18] Similar changes in [11]B chemical shift have been noted in related systems on moving between Rh(I) and Rh(III) oxidation states.[19,21] The $^{31}P\{^1H\}$ NMR spectrum shows a single environment δ 26.7 [d, $J(RhP) = 182$ Hz]. The solid-state structure of complex **3** supports the solution data (Fig. 1), in particular a close Rh···B distance of 2.179(7) Å, which is the same within error to that found in **2**, 2.162(5) Å,[18] and the formation of the linear hydroboration product. Complexes such as **2** and **3** are valence isoelectronic analogs of sigma alkane complexes,[22–24] while related alkyl sigma amine–borane complexes have previously been prepared.[25]

With complexes **2** and **3** in hand the catalytic hydroboration of TBE with $H_3B\cdot NMe_3$ was explored using these as precatalysts (Scheme 3). As previously reported,[18] complex **2** (5 mol%) catalyses the complete conversion to $H_2B(CH_2CH_2{}^tBu)\cdot NMe_3$ (**I**)

Scheme 2 Formation of **2** (E = C) and **3** (E = Si). $[BAr^F_4]^-$ anions not shown.

$[2]$ 5 mol %, 3 hour, 100 %
$[2]$ or $[3]$ 0.5 mol %, 12 hour, 85 %

Scheme 3 Rhodium-catalysed hydroboration of TBE by $H_3B\cdot NMe_3$.

This journal is © The Royal Society of Chemistry 2014

Catal. Sci. Technol., 2014, **4**, 3486–3494 | **3487**

from TBE and $H_3B \cdot NMe_3$ within 3 hours. The catalysis was conducted with a 2:1 ratio of alkene:$H_3B \cdot NMe_3$ as the {Rh(xantphos)}$^+$ fragment has been reported to promote the slow dehydrogenative homocoupling of $H_3B \cdot NMe_3$ to form [Rh($\kappa^2$$_{P,P}$-xantphos)($\eta^2$-$H_4B_2 \cdot 2NMe_3$)][BAr$^F_4$] (4) alongside 1 (Scheme 4),[18] and a two-fold excess of alkene prevents the formation of 4 in detectable quantities (*vide infra*). During catalysis, complex 2 was the only observed resting state by ^1H and $^{31}P\{^1H\}$ NMR spectroscopy.[26] The ^1H NMR spectrum of isolated I confirms anti-Markovnikov regioselectivity, with two, integral 2H, multiplets at δ 1.42 and δ 0.55 assigned to the methylene groups. The ^{11}B NMR spectrum shows a triplet at δ −0.83 [J(BH) = 96 Hz].[14]

Kinetic studies

Given the promising rate of hydroboration of TBE with catalyst 2 to afford I, the catalyst loading was reduced to 0.5 mol%, relative to $H_3B \cdot NMe_3$. Under these conditions ([$H_3B \cdot NMe_3$] = 0.19 M, [TBE] = 0.38 M, 1,2-$F_2C_6H_4$ solvent), consumption of $H_3B \cdot NMe_3$ to yield I proceeded to 85% completion after 12 hours as monitored by ^{11}B NMR spectroscopy, with the balance being made by unreacted $H_3B \cdot NMe_3$.

Scheme 4 Formation of complex 4 from addition of excess $H_3B \cdot NMe_3$ to 2. [BAr$^F_4$]$^-$ anions not shown.

Longer reaction times did not result in further reaction, suggesting either product inhibition and/or catalyst decomposition. When starting from precatalyst 3 a very similar overall temporal profile was observed, suggesting the identity of the initially bound amine–borane (I or II) does not affect the overall rate of catalysis.

The potential for product inhibition,[14] and the parallel homocoupling reaction with excess $H_3B \cdot NMe_3$, suggested that the method of initial rates was most appropriate to probe the reaction orders with respect to substrates and the catalyst.[27] After 300 s at 5 mol% loading of 3 *ca.* 50% substrate conversion had occurred, while at 0.5 mol% this was now only *ca.* 10% conversion, making the lower loading suitable for study by the initial rate method. We further chose to study catalyst 3 as this would also give additional information as to the evolution of the likely resting states. Table 1 presents the data from this study, and Fig. 2 presents some of these data in graphical format.

Comparison of entries 1, 2 and 3 (Fig. 2a) show that the reaction is essentially first order in [TBE]. Entries 1 and 4 demonstrate a first order relationship in catalyst 3 (Fig. 2b). Entries 2, 5 and 6 show that increasing the concentration of [$H_3B \cdot NMe_3$] moves from an approximate first order relationship to an inhibition of catalysis at higher concentrations of amine–borane (Fig. 2c), we presume as homocoupling to form 4 becomes competitive. In complex 4, the diborane(4) is relatively strongly bound to the metal centre, remaining intact even with the addition of MeCN,[18] and thus is unlikely to be as active in catalysis. Indeed, use of 4 as a catalyst (0.5 mol%) resulted in reduced turnover. Addition of excess product I (~70 equivalents, entry 7) results in a significant slowing of the initial rate, consistent with strong product inhibition,

Table 1 Initial rates obtained from variation of concentration of 3, $H_3B \cdot NMe_3$ and TBE, 295 K, 1,2-$F_2C_6H_4$ solvent

Entry	[3] (10^{-4} M)	[$H_3B \cdot NMe_3$] (M)	[TBE] (M)	Initial rate^a (10^{-5} M s^{-1})
1	9.5	0.19	0.38	6.81 ± 0.12
2	9.5	0.19	0.19	3.64 ± 0.27
3	9.5	0.19	0.76	12.98 ± 0.38
4	19.0	0.19	0.38	13.25 ± 0.56
5	9.5	0.38	0.19	7.41 ± 0.53
6	9.5	0.76	0.19	6.33 ± 0.40
7^b	9.5	0.19	0.38	2.07 ± 0.11
8	[2] 9.5	0.19	0.38	7.44 ± 0.64
9	9.5	0.19^c	0.38	5.09 ± 0.07

^{a} Calculated from the pseudo zero-order region of the temporal evolution of I as measured by ^{11}B NMR spectroscopy over the first 300 s of catalysis. ^{b} With an additional 70 equiv. I at the start of catalysis. ^{c} Using $D_3B \cdot NMe_3$ instead of $H_3B \cdot NMe_3$.

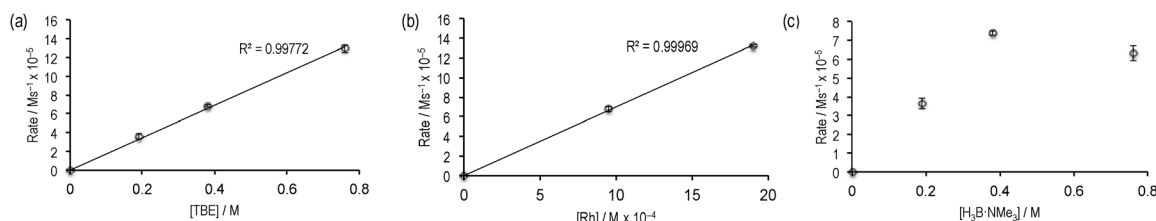**Fig. 2** Initial rate experiments: (a) variation of [TBE]; (b) variation of [3]; (c) variation of $H_3B \cdot NMe_3$. See Table 1 for more details.

3488 | *Catal. Sci. Technol.*, 2014, **4**, 3486–3494

This journal is © The Royal Society of Chemistry 2014

as observed to a lesser degree with the $[Rh(P^iBu_2{}^tBu)_2][BAr^F_4]$ system.[14] Catalyst **3** and catalyst **2** operated at the same initial rate, within error (entries 1 and 8), suggesting that the identity of the bound primary borane (*i.e.* **I** or **II**) does not influence initial rate of turnover.

Hydroboration of TBE and $H_3B \cdot NMe_3$ catalysed using **3** enables more information to be gleaned about possible resting states. At 0.5 mol% loading, the catalyst concentration is too low to be observable by NMR spectroscopy under the conditions used. However, at 5 mol% loading the rhodium-containing species can be probed by ^1H and $^{31}P\{^1H\}$ NMR spectroscopy. The diagnostic, broad, hydride signals for **2** and **3** appear at similar chemical shifts in $1,2\text{-}F_2C_6H_4$ solvent [δ -6.85[18] and δ -6.54 respectively]. In the early stages of catalysis (~20% conversion), the ^1H NMR spectrum shows a mixture of **2** and **3**, evident by broad overlapping hydride peaks. As catalysis progresses, this broad overlapping resonance sharpens and **2** becomes the dominant species demonstrating that **I** displaces **II** in the resting state during catalysis. Under the conditions of excess $H_3B \cdot NMe_3$ (*cf.* entry 6), using 5 mol% **3** to enable monitoring by ^1H NMR spectroscopy, complex **4** grows in over time, whereas under conditions of excess TBE it is not observed. This is consistent with the kinetic data that suggest removal from the system of active catalyst at high $[H_3B \cdot NMe_3]$, leading to inhibition.

The change in resting state from **3** to **2** has also been probed using electrospray ionization mass spectrometry (ESI-MS) using the pressurised sample infusion (PSI) technique.[28–30] The particular advantage of this technique is that it allows for very high data density over a wide dynamic range, and is thus ideal for analysing evolving mixtures during catalysis. Fig. 3 shows the temporal profile of the catalysis using **3**. This experiment was run at 15 mol%, which was determined to be the best conditions for the optimal (low) concentration necessary for PSI-ESI-MS. Immediately at the start of catalysis the resting state moves from **3** to **2**, consistent with the NMR experiments. These ESI-MS experiments also reveal the presence, at early stages of the reaction of three other species. The first is
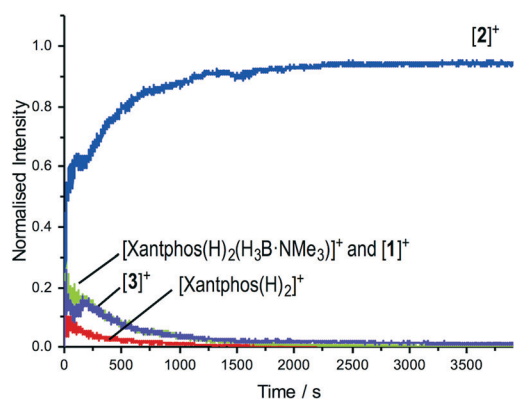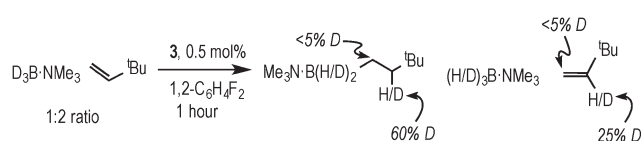
identified as $[Rh(xantphos)(H_3B \cdot NMe_3)]^+$, ($m/z$ = 754.24; calc. 754.20), although we cannot comment on the precise structure: it could be a Rh(I) sigma-bound amine–borane complex, or a Rh(III) B–H activated hydrido-boryl. Both structural forms have precedent[19,31] and are likely to be in equilibrium with one another.[32] Indeed both have been calculated to be accessible, but thermodynamically unfavoured, compared with **2**.[18] $[Rh(xantphos)(H_2)]^+$ (m/z = 683.15; calc. 683.11) and $[\mathbf{1}]^+$ are also observed, which we suggest both come from a small amount of $[\mathbf{1}]^+$ formed parallel with **4** during catalysis (Scheme 4). That we do not observe any of these species by ^1H NMR spectroscopy (hydride region) suggests that ESI-MS is particularly sensitive to their observation. These species decay at a very similar rate to $[\mathbf{3}]^+$, which suggests that the build-up of **I** during catalysis pushes any equilibria operating to favour of **2**. This observation is also consistent with product inhibition from initial rate experiments.

Labelling studies

Complex **3** (and **2**) are initially produced under conditions of excess alkene (Scheme 2), suggesting that the alkene does not bind competitively with **II** (or **I**), while the dependence of the rate law upon both [TBE] and $[H_3B \cdot NMe_3]$ indicates that *irreversible* B–H oxidative addition prior to alkene coordination is not rate-determining. The potential for reversibility of the binding of both $H_3B \cdot NMe_3$ and TBE to the metal centre was further probed using $D_3B \cdot NMe_3$ instead of $H_3B \cdot NMe_3$ during catalysis. Initial rate experiments (Table 1, entry 9) showed a KIE of 1.34 ± 0.04, consistent with irreversible B–H activation not being rate determining. However, due to the H/D exchange observed between the amine–borane and alkene (*vide infra*) interpretation of the absolute magnitude of this measurement should be treated with a degree of caution.

After 1 hour of catalysis under conditions of excess alkene (28% conversion, Scheme 5) ^2H NMR spectroscopy showed incorporation of deuterium into the internal position of the free, unreacted, alkene (δ 5.89), while the corresponding signal in the ^1H NMR spectrum decreased by *ca.* 25% relative to the other alkene signals at δ 4.99 and 4.89. This demonstrates that H/D exchange occurs only occurs at the internal alkene proton. H/D exchange in free amine–borane was evidenced by the ^{11}B NMR spectrum that at early stages of catalysis showed a broad peak corresponding to $D_3B \cdot NMe_3$ and evolved with time to show significant signs of B–H coupling.[33] The final product $d\text{-}\mathbf{I}$ showed no H/D exchange

Fig. 3 ESI-MS under PSI conditions[29] of the reaction of TBE with $H_3B \cdot NMe_3$ catalysed by **3**. Conditions: $H_3B \cdot NMe_3$, 0.006 M, TBE 0.013 M; [**3**] 0.001 M, $1,2\text{-}F_2C_6H_4$. Under these conditions of concentration and experiment catalysis proceeded to 80% conversion.

Scheme 5 The products observed after 1 hour of catalysis using $D_3B \cdot NMe_3$. Conditions: $[D_3B \cdot NMe_3]$ = 0.19 M, [TBE] = 0.38 M, $1,2\text{-}F_2C_6H_4$, 0.5 mol% **3**.

α- to the borane, and ~40% H/D exchange at the β position (*i.e.* 60% D).

These data suggest that coordination of $H_3B \cdot NMe_3$, B–H activation, coordination and insertion of the alkene into the Rh–H bond are all reversible, to ultimately give the linear product. Moreover the lack of H/D exchange in the final product at the α-position, *and* a similar lack of exchange in the terminal positions of the free alkene, suggests that insertion to form the branched product is not occurring. We also suggest that hydride migration to the alkene, rather than boryl migration to form an intermediate such as **F** (Scheme 6), is by far dominant.[34] Intermediates such as **F** have been postulated in dehydrogenative borylation reactions,[5,8,35,36] the products of which are not observed here. Although we cannot fully discount that boryl migration from **F** is reversible but the barrier to reductive elimination from **F** is high, we consider that this scenario is less likely based upon literature precedent.[6–8,35]
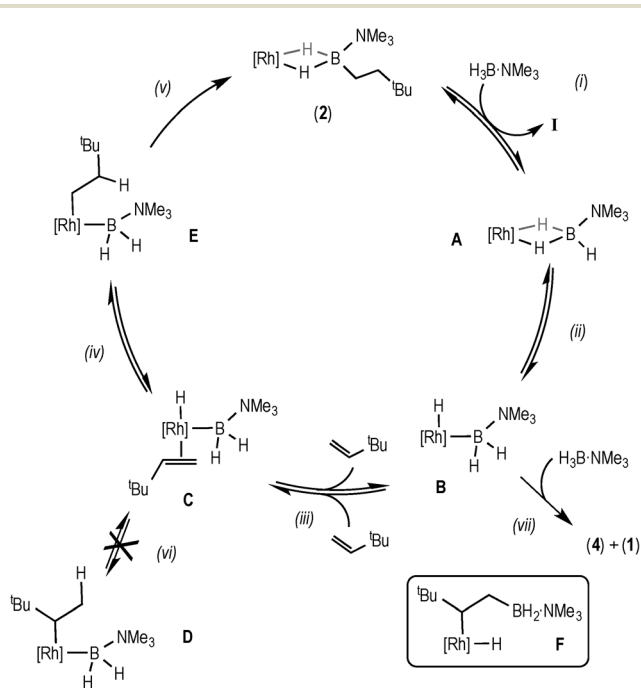
Bringing these data and observations together leads us to propose the catalytic pathway shown in Scheme 6 for the hydroboration of TBE using $H_3B \cdot NMe_3$ and **3**. This pathway is similar to that reported for using the $[Rh(P^iBu_2{}^iPr)_2]^+$ catalyst system,[14] as well as late transition metal hydroboration systems that use, for example, HBCat.[3,5,6,8]

The elementary steps in this cycle are thus: complex **2** does not react with TBE but undergoes reversible B–H activation with $H_3B \cdot NMe_3$, (i) and (ii), as shown by H/D exchange into free $D_3B \cdot NMe_3$ during the early phases of catalysis. Monitoring by ESI-MS shows a species consistent with **A** or **B** (m/z = 754.24) before **2** becomes the only species observed. TBE binding and insertion into Rh–H is reversible, (iii), as
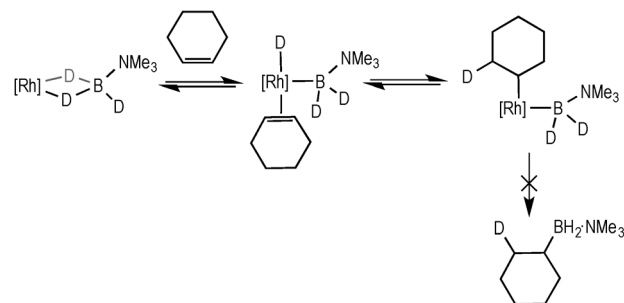
demonstrated by H/D exchange into the free alkene during catalysis. No branched product is observed[37] and no H/D exchange at the α-position of the linear product is measured, showing that insertion from **C** to form **D** (vi) is neither kinetically competent nor reversible. Insertion from **C** to give the linear intermediate **E** is reversible (iv), as there is significant (40%) H/D exchange at the β-position in the final product, as well as into the free alkene when $D_3B \cdot NMe_3$ is used, that suggests that β-H-elimination from **E** occurs. Overall these H/D labelling experiments suggest that reductive elimination (v) is the turnover-limiting step during the early stages of catalysis. As reductive elimination would be expected to have a small (close to unity) KIE, the modest measured value might reflect a system at equilibrium before the turnover limiting step (as postulated), *i.e.* an equilibrium isotope effect.[38]

Hydroboration of alkenes other than TBE

Under stoichiometric conditions the hydroboration of alkenes other than TBE was explored. With the hindered alkene 2,3-dimethyl-2-butene (2 equiv.) no evidence of hydroboration using $1/H_3B \cdot NMe_3$ was observed, with **1** remaining the major organometallic species in solution over an hour. After 24 hours, a 2 : 1 mixture of **1** and **4** were present, suggesting that the B–B homocoupling was occurring. Cyclohexene behaved similarly, as previously reported, with no hydroboration observed; instead it promotes loss of H_2 from **1**, driving the formation of **4**.[18] To probe the possibility of non-productive coordination of cyclohexene at the metal centre, a mixture of $D_3B \cdot NMe_3$ (0.19 M), cyclohexene (0.38 M) and **3** (5 mol%, relative to $D_3B \cdot NMe_3$) was monitored by ^2H NMR spectroscopy. This showed, as well as deuterium incorporation into signals for cyclohexane that arise from deuteration of **1** (δ 1.58 and δ 1.43), incorporation of deuterium into the alkene signal (δ 5.89) after 90 minutes (Scheme 7). These data suggest that reversible alkene coordination and deuteride insertion can occur to give an intermediate similar to **E**; while the lack of hydroborated product suggests that the reductive elimination, as proposed to be the rate determining step for catalysis with TBE, is slow compared with overall dehydrogenative homocoupling from an intermediate **B** to form **4**. This is presumably related to the relative rates of reductive C–B coupling of primary and secondary alkyl–boryls, which in turn is likely related to barriers

Scheme 6 Proposed mechanism for the catalytic hydroboration using data from the early phase of catalysis. [Rh] = [Rh(xantphos)]⁺.

Scheme 7 Reversible deuterio-insertion with cyclohexene.

3490 | *Catal. Sci. Technol.*, 2014, **4**, 3486–3494

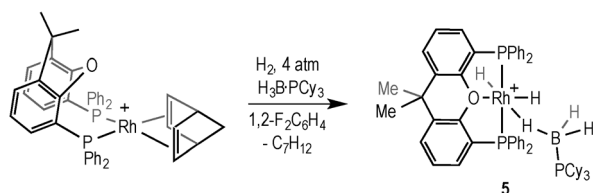This journal is © The Royal Society of Chemistry 2014

to re-orientation of the sp^3 alkyl and boryl groups prior to reductive coupling,[39] which is expected to be greater for locally bulkier substituents. Thus TBE undergoes hydroboration, while cyclohexene does not.

With 1-hexene, catalysis (5 mol% of **3** relative to H$_3$B·NMe$_3$) reached 37% conversion after 30 minutes yielding a product consistent with Me(CH$_2$)$_5$H$_2$B·NMe$_3$, as shown by a triplet [J(HB) = 91 Hz] in the ^{11}B NMR spectrum at δ −1.4, although we were not able to isolate this material pure and thus cannot comment on the linear : branched ratio. After 1 week, a maximum conversion of 63% is reached. However, significant decomposition of the catalyst was observed, for which we cannot definitively provide a structure derived from the spectroscopic data. Thus, the hydroboration of alkenes with **3** appears to work best with TBE, with other alkenes only of limited utility.
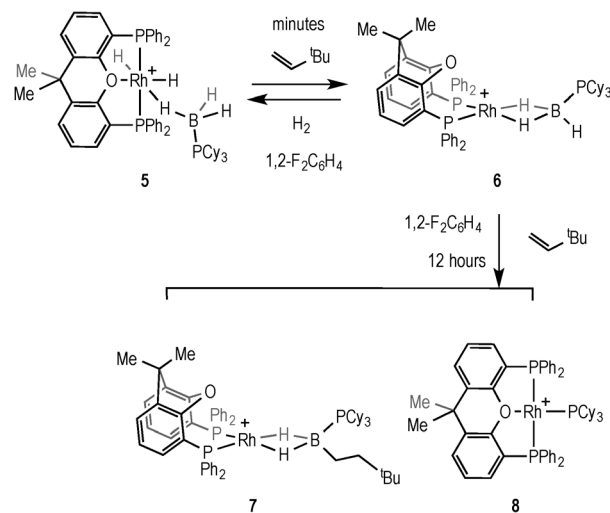
Hydroboration with phosphine–boranes

The addition of H$_2$ to [Rh(xantphos)(NBD)][BAr$^F_4$] (NBD = norbornadiene) in the presence of the tertiary phosphine–borane H$_3$B·PCy$_3$ afforded [Rh($\kappa^3_{P,O,P}$-xantphos)(H)$_2$(η^1-H$_3$B·PCy$_3$)][BAr$^F_4$] (**5**) in quantitative yield by NMR spectroscopy (Scheme 8). Complex **5** was characterised *in situ* using NMR spectroscopy, and presents very similar data to the analogous complex **1**.[18] It is also related to the sigma phosphine–borane complex [Ru(xantphos)(H)(PPh$_2$H)(H$_3$B·PPh$_2$H)][BAr$^F_4$].[40] The ^{1}H NMR spectrum shows 3 hydride environments in a 3 : 1 : 1 ratio, consistent with the phosphine–borane bound in an η^1 fashion that is undergoing rapid exchange between B–H–Rh and B–H groups, and two mutually *cis* hydrides: δ −1.42 [br, BH$_3$, sharpens on ^{11}B decoupling], δ −14.62 [br dtd, RhH] and δ −19.13 [dtd, RhH]. Two ^{31}P environments are observed in the ^{31}P{^{1}H} NMR spectrum at δ 41.8 [d, J(RhP) = 114 Hz] and δ 20.1 (br, PCy$_3$) in a 2 : 1 ratio respectively. Attempts to crystallise **5** were unsuccessful, resulting in decomposition.

Addition of 2 equivalents of TBE to pale yellow **5** resulted in the formation of a dark green solution of a new compound formulated as [Rh($\kappa^2_{P,P}$-xantphos)(η^2-H$_3$B·PCy$_3$)][BAr$^F_4$] (**6**), Scheme 9, in quantitative yield by NMR spectroscopy. Removal of volatiles allowed the isolation of **6** as a dark green solid. The NMR data for **6** are consistent with η^2 binding of the phosphine–borane; in the ^{1}H NMR spectrum, a quadrupolar broadened, integral 3H signal is observed at δ −2.38, which sharpens on ^{11}B decoupling, while the ^{11}B NMR spectrum shows a broad signal at δ −3.0. The ^{31}P{^{1}H} NMR spectrum is also consistent with a Rh(I) phosphine–borane complex, with two signals observed at δ 28.9 [d, J(RhP) = 190 Hz] and δ 17.3

Scheme 9 Formation of **6**, **7** and **8**. [BAr$^F_4$]$^-$ anions are not shown.

(br, PCy$_3$). These data are consistent with those reported for other [Rh(chelating phosphine)(H$_3$B·PR$_3$)]$^+$ complexes.[41] Addition of H$_2$ (4 atm) to a CD$_2$Cl$_2$ solution of **6** reforms complex **5** in quantitative yields by NMR spectroscopy. Degassing a CD$_2$Cl$_2$ solution of **5** and placing under static vacuum for 4 hours resulted in an approximately 1 : 1 ratio of **5** : **6**, suggestive of an equilibrium between the two species. Interestingly, for the [Rh(xantphos)]$^+$ fragment we cannot isolate, or observe by NMR spectroscopy, the equivalent Rh(I) H$_3$B·NMe$_3$ complex to **6**, as **4** forms instead from homocoupling.[18]

The ability of **6** to mediate hydroboration was probed by addition of excess (2.5 equiv.) TBE in 1,2-F$_2$C$_6$H$_4$ solvent, by addition of the alkene to *in situ* generated **6**, Scheme 9. After 45 minutes a new peak is apparent in the ^{1}H NMR spectrum at δ −5.58 that is assigned to an Rh–HB interaction, consistent with the slow formation of [Rh($\kappa^2_{P,P}$-xantphos)(η^2-H$_2$B(CH$_2$CH$_2{}^t$Bu)·PCy$_3$)][BAr$^F_4$] (**7**), similar to **2** and **3**. After 16 hours the ratio of **7** had increased relative to **6** (~5 : 1 7:6). However small amounts (*ca.* 5% by ^{31}P{^{1}H} NMR spectroscopy) of a parallel product resulting from P–B cleavage [Rh($\kappa^3_{P,O,P}$-xantphos)(PCy$_3$)][BAr$^F_4$] (**8**) were also observed by ^{31}P{^{1}H} NMR spectroscopy at δ 61.3 [dt, J(RhP) = 192, J(PP) = 34 Hz] and δ 37.8 [dd, J(RhP) = 155, J(PP) = 34 Hz]. P–B bond cleavage has been noted previously during metal-catalysed dehydrocoupling of phosphine–boranes.[40,42,43] After a further 12 hours all of **6** was consumed, but a greater proportion of **8** (*ca.* 33%) was also present. Recrystallisation of the reaction mixture after several hours afforded a small crop of green crystals of **7** suitable for X-ray diffraction, and although the resulting data quality was poor and only the gross connectivity can thus be discussed, the solid-state structure of **7** suggests anti-Markovnikov hydroboration, as with **2** and **3** (see ESI†). The bulk composition could not be reliably determined by NMR spectroscopy as the alkyl region of the ^{1}H NMR spectrum is dominated by the cyclohexyl peaks from the mixture of **6** and **8**.

From such mixtures, several orange crystals of **8** also grew, confirming its solid-state structure (Fig. 4) as a square planar
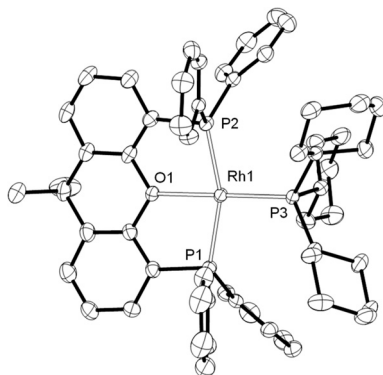

Scheme 8 Formation of complex **5**. [BAr$^F_4$]$^-$ anion not shown.

This journal is © The Royal Society of Chemistry 2014

Catal. Sci. Technol., 2014, **4**, 3486–3494 | **3491**

Fig. 4 Solid state structure of the cationic portion of **8**. [BAr$^F_4$]$^-$ anion and H atoms are omitted for clarity. Displacement ellipsoids are drawn at the 50% probability level. Selected bond lengths (Å) and angles (°): Rh1–P1, 2.2854(7); Rh1–P2, 2.2923(7); P3–Rh1, 2.2611(7); Rh1–O1, 2.2395(19); P2–Rh1–P1, 159.70(3); P3–Rh1–O1, 170.44(6).

Rh(I) complex [sum of angles around Rh = 361.5°] with xantphos coordinated in a *mer* manner, similar to the closely related [Rh(κ$^3_{P,O,P}$-xantphos)(PCyp$_3$)][BAr$^F_4$] (Cyp = cyclopentyl),[44] and [Rh(κ$^3_{P,O,P}$-xantphos)(CO)][BF$_4$].[45] Complex **8** has been independently synthesised from addition of PCy$_3$ to **2** (see Experimental).

Conclusions

We have described that the [Rh(xantphos)]$^+$ fragment acts as an effective catalyst for the hydroboration of TBE using the amine–borane H$_3$B·NMe$_3$ at low (0.5 mol%) catalyst loadings. Investigations into the mechanism using the initial rate method and labelling studies show that reductive elimination of the linear hydroboration product is likely the rate-limiting step at the early stages of catalysis. This system is not as effective for other alkenes such as 1-hexene, or using the phosphine–borane H$_3$B·PCy$_3$; with decomposition or P–B bond cleavage occurring respectively.

Experimental section

All manipulations, unless otherwise stated, were performed under an argon atmosphere using standard Schlenk and glove-box techniques. Glassware was oven dried at 130 °C overnight and flamed under vacuum prior to use. Pentane, hexanes, CH$_2$Cl$_2$ and MeCN were dried using a Grubbs type solvent purification system (MBraun SPS-800) and degassed by successive freeze–pump–thaw cycles. 1,2-F$_2$C$_6$H$_4$ (pre-treated with alumina) and CD$_2$Cl$_2$ were dried over CaH$_2$, vacuum distilled and stored over 3 Å molecular sieves. H$_3$B·NMe$_3$ was purchased from Aldrich and sublimed prior to use (5 × 10^{-2} Torr, 298 K). Cyclohexene, trimethylvinyl silane (TVMS), and 3,3-dimethyl-1-butene (TBE) were purchased from Aldrich, dried over sodium, vacuum distilled and stored over 3 Å molecular sieves. [Rh(xantphos)(NBD)][BAr$^F_4$] was prepared by the literature method.[46] NMR spectra were

recorded on a Bruker AVIII-500 spectrometer at room temperature, unless otherwise stated. In 1,2-F$_2$C$_6$H$_4$, ^{1}H NMR spectra were pre-locked to a sample of C$_6$D$_6$ (25%) and 1,2-F$_2$C$_6$H$_4$ (75%) and referenced to the centre of the downfield solvent multiplet, δ = 7.07. ^{31}P and ^{11}B NMR spectra were referenced against 85% H$_3$PO$_4$ (external) and BF$_3$·OEt$_2$ (external) respectively. Chemical shifts (δ) are quoted in ppm and coupling constants (J) in Hz. ESI-MS were recorded on a Bruker MicrO-TOF instrument interfaced with a glove-box,[28] or using the PSI-ESI technique as described previously,[29,30] and in detail below. Microanalyses were performed by Elemental Micro-analysis Ltd.

ESI-MS reaction monitoring using pressurized sample infusion

A Schlenk flask under nitrogen containing **3** (4.7 mg, 0.0028 mmol) and H$_3$B·NMe$_3$ (1.4 mg, 0.019 mmol) was pressurised to 1.5 psi using 99.998% purity argon gas and connected to the mass spectrometer *via* a short length of PEEK tubing. A solution of TBE (4.8 μL, 0.038 mmol) in 1,2-F$_2$C$_6$H$_4$ (3 mL) was injected into the pressurized Schlenk flask through a septum and collection on the mass spectrometer was initiated. Mass spectra were collected on a Micromass Q-Tof micro mass spectrometer in positive ion mode using pneumatically assisted electrospray ionization: capillary voltage, 2900 V; sample cone voltage, 15 V; extraction voltage, 0.5 V; source temperature, 92 °C; desolvation temperature, 192 °C; cone gas flow, 100 L h^{-1}; desolvation gas flow, 200 L h^{-1}; collision voltage, 2 V; MCP voltage, 2400 V. No smoothing of the data was performed. Aliquots of the reaction mixture were removed *via* syringe during the reaction for analysis by ^{11}B NMR spectroscopy.

General procedure for catalytic hydroboration

The alkene and 1,2-F$_2$C$_6$H$_4$ (0.6 mL) were mixed in a Young's NMR tube and transferred to a new NMR tube containing **2** or **3** and H$_3$B·NMe$_3$. The samples were immediately frozen in liquid N$_2$, and monitored *in situ* by ^{11}B NMR spectroscopy on warming. See Table 1 for more details of relative concentrations.

Synthesis and characterisation of new complexes

Synthesis of [Rh(κ$^2_{P,P}$-xantphos)(η^2-H$_2$B(CH$_2$CH$_2$SiMe$_3$)·NMe$_3$)][BAr$^F_4$] (3). [Rh(xantphos)(nbd)][BAr$^F_4$] (100 mg, 0.06 mmol) and H$_3$B·NMe$_3$ (4.4 mg, 0.06 mmol) were dissolved in 1,2-F$_2$C$_6$H$_4$ in a Young's flask, the contents immediately frozen in liquid N$_2$, and the argon headspace replaced with H$_2$ (*ca.* 4 atm), yielding **1** *in situ* upon warming to room temperature. The flask was degassed (3 freeze–pump–thaw cycles), opened to an argon atmosphere, and TMVS (40 μL, 0.272 mmol) was added. The solution turned from pale yellow to dark green. After 10 minutes, the volatiles were removed *in vacuo*, and the solid was washed twice with pentane (2 × 5 mL) with sonication. The solid was dried *in vacuo*, affording a blue/green powder, mass 86 mg (82% yield). Crystals suitable for X-ray diffraction were grown from recrystallisation from 1,2-F$_2$C$_6$H$_4$ and pentane at −30 °C. ^{1}H NMR (500 MHz, 1,2-F$_2$C$_6$H$_4$): δ 8.33 (s, 8H,

[BArF$_4$]$^-$), 7.69 (s, 4H, [BArF$_4$]$^-$), 2.61 (s, 9H, NMe$_3$), 1.73 (s, 3H, xantphos CH$_3$), 1.67 (s, 3H, xantphos CH$_3$), 1.17 (m, 2H, CH$_2$SiMe$_3$), 0.78 (br m, 2H, CH$_2$BH$_2$NMe$_3$), 0.06 (s, 9H, SiMe$_3$), −6.54 (br, 2H, BH$_2$). The peak at δ −6.54 sharpens into an overlapping doublet of doublets (virtual triplet) upon decoupling to ^{11}B [J(RhH) = 36 and J(PH) = 36 Hz]. Signals from the xantphos aryl ligand were not observed, presumably obscured by the solvent. ^{29}Si-^{1}H HMBC NMR (500 MHz, 1,2-F$_2$C$_6$H$_4$): correlation observed between silicon at δ 2.1 and protons at δ 1.17 and 0.06. ^{31}P{^{1}H} NMR (202 MHz, 1,2-F$_2$C$_6$H$_4$): δ 26.7 [d, J(RhP) = 182 Hz]. ^{11}B NMR (160 MHz, 1,2-F$_2$C$_6$H$_4$): δ 37 (br, BH$_2$), −6.2 (s, [BArF$_4$]$^-$). ESI-MS (1,2-F$_2$C$_6$H$_4$, 60 °C, 4.5 kV): m/z 854.28 [M]$^+$ (calc. 854.28). Peak displays the expected isotopic pattern. Elemental microanalysis: calc. RhP$_2$OC$_{79}$H$_{68}$B$_2$F$_{24}$NSi (1717.94 g mol^{-1}): C, 55.23; H, 3.99; N, 0.82. Found: C, 55.16; H, 4.03; N, 0.88.

Synthesis of [Rh($\kappa^3$$_{P,O,P}$-xantphos)(H)$_2$($\eta^1$-H$_3$B·PCy$_3$)][BArF$_4$] (5). [Rh(xantphos)(nbd)][BArF$_4$] (20 mg, 0.01 mmol) and H$_3$B·PCy$_3$ (2.5 mg, 0.01 mmol) were dissolved in 1,2-F$_2$C$_6$H$_4$ in a high pressure NMR tube, the contents immediately frozen in liquid N$_2$, and the argon headspace replaced with H$_2$ (ca. 4 atm), yielding **5** in situ upon warming to room temperature and shaking. **5** could not be isolated due to loss of dihydrogen upon removal from the H$_2$ atmosphere. Attempts to recrystallise under H$_2$ resulted in impure oil, as measured by NMR spectroscopy. However, the following NMR spectroscopic data were obtained from the hydrogenation of preformed **6**. ^{1}H NMR (500 MHz, CD$_2$Cl$_2$): δ 8.10–7.27 (m, 26H, xantphos aryl signals), 7.73 (s, 8H, [BArF$_4$]$^-$), 7.56 (s, 4H, [BArF$_4$]$^-$), 2.05–0.81 (m, 39H, overlapping Cy and xantphos CH$_3$ signals), −1.63 (br, 3H, BH$_3$), −14.80 (br, 1H, RhH), −19.40 (br, 1H, RhH). ^{1}H NMR (500 MHz, CD$_2$Cl$_2$, 200 K, selected data): δ 1.87 (s, 3H, xantphos CH$_3$ signal), 1.47 (s, 3H, xantphos CH$_3$ signal), −14.34 (br m, 1H, RhH), −19.40 [br dtd, J(RhH) = 26, J(PH) = 14, J(HH) = 7 Hz, RhH]. ^{31}P{^{1}H} NMR (202 MHz, CD$_2$Cl$_2$): δ 41.8 [d, J(RhP) = 116 Hz], 20.2 (br, PCy$_3$). ^{11}B NMR (160 M Hz, CD$_2$Cl$_2$): δ −6.6 (s, [BArF$_4$]$^-$), −43.5 (br, BH$_3$).

Synthesis of [Rh($\kappa^2$$_{P,P}$-xantphos)($\eta^2$-H$_3$B·PCy$_3$)][BArF$_4$] (6). **5** (55 mg, 0.03 mmol) was formed in situ under H$_2$ (4 atm) in a Young's crystallisation flask. The flask was degassed (3 freeze–pump–thaw cycles), opened to an argon atmosphere, and TBE (8 μL, 0.06 mmol) was added. The solution turned from pale yellow to dark green. After 5 minutes, the volatiles were removed in vacuo to prevent onward reactivity, and washed twice with pentane (3 mL) with sonication. The resulting oily solid was redissolved in the minimum amount of 1,2-F$_2$C$_6$H$_4$ and layered with pentane, affording green needle-like crystals (not suitable for X-ray diffraction) at −30 °C. Mass 40 mg (73% yield) ^{1}H NMR (500 MHz, CD$_2$Cl$_2$): δ 7.73 (s, 8H, [BArF$_4$]$^-$), 7.56 (s, 4H, [BArF$_4$]$^-$), 7.64–6.40 (m, 26H, xantphos aryl signals), 1.86–1.08 (m, 39H, PCy$_3$ and xantphos CH$_3$ signals), −2.38 (br, 3H, BH$_3$). Upon decoupling to ^{11}B, the signal at −2.38 sharpens. ^{31}P{^{1}H} NMR (202 MHz, CD$_2$Cl$_2$): δ 28.9 [d, J(RhP) = 190 Hz], 17.3 (br, PCy$_3$). ^{11}B NMR (160 M Hz, CD$_2$Cl$_2$): δ −3.0 (br, BH$_3$), −6.6 (s, [BArF$_4$]$^-$). ESI-MS (1,2-F$_2$C$_6$H$_4$, 60 °C, 4.5 kV) was attempted but decomposition resulted under these

conditions. Elemental microanalysis: calc. RhP$_3$OC$_{89}$H$_{80}$B$_2$F$_{24}$ (1839.03 g mol^{-1}): C, 58.13; H, 4.38. Found: C, 57.43; H, 4.59.

Attempted synthesis of [Rh($\kappa^2$$_{P,P}$-xantphos)($\eta^2$-H$_2$B (CH$_2CH_2$^{t}Bu)·PCy$_3$)][BArF$_4$] (7). Complex **5** (0.02 mmol) was formed in situ under H$_2$ (4 atm) in a Young's crystallisation flask as described above. The flask was degassed (3 freeze–pump–thaw cycles), opened to an argon atmosphere, and TBE (7 μL, 0.05 mmol) was added. The solution turned from pale yellow to dark green, as complex **6** is formed immediately. Upon leaving the mixture for 45 minutes, a mixture of **6** and **7** are present. Standing for longer periods (12 hours) resulted in a decreased amount of **6**, and a new complex, **8**, was now observed (see below for an independent synthesis of **8**). Due to this mixture, our attempts to isolate pure **7** were unsuccessful. A small number of green single crystals suitable for diffraction were obtained by leaving the reaction mixture for several hours to form a mixture of **6** and **7**, layering the solution with pentane and storing at −30 °C. Analysis by NMR spectroscopy of these crystals dissolved in CD$_2$Cl$_2$ indicated a mixture of **6** and **7**. Due to the mixture, only selected NMR data for **7** are available as the alkyl and aryl regions are obscured by **6** signals. ^{1}H NMR (500 MHz, CD$_2$Cl$_2$): δ −5.92 (br, Rh–H$_2$B). The signal sharpens into an overlapping doublet of doublets (virtual triplet) upon decoupling to ^{11}B [J(RhH) = 33 and J(PH) = 33 Hz]. ^{31}P{^{1}H} NMR (202 MHz, CD$_2$Cl$_2$): δ 29.5 [d, J(RhP) = 190 Hz], 8.8 (br, PCy$_3$). ^{11}B NMR (160 M Hz, CD$_2$Cl$_2$): δ 18.5 (br, BH$_3$), −6.6 (s, [BArF$_4$]$^-$). ESI-MS (1,2-F$_2$C$_6$H$_4$, 60 °C, 4.5 kV) was attempted but decomposition resulted under these conditions. Upon repeating the reaction a small number of orange crystals of **8** formed which could be mechanically separated from green **6** and **7**, whose spectroscopic data match that from independently synthesised **8** (see below).

Synthesis of [Rh($\kappa^3$$_{P,O,P}$-xantphos)(PCy$_3$)][BArF$_4$] (8). 1,2-F$_2C_6H_4$ (0.4 mL) was added to **2** (17 mg, 0.010 mmol) and PCy$_3$ (0.011 mmol) in a small Schlenk flask. The colour changed from blue to orange immediately on mixing. The solvent was removed in vacuo, and the remaining orange oil was washed three times with pentane (2 mL) with sonication. Stirring under vacuum afforded an orange powder, mass 13 mg (71% yield). ^{1}H NMR (500 MHz, CD$_2$Cl$_2$): δ 7.72 (s, 8H, [BArF$_4$]$^-$), 8.05–7.71 (m, 30H, xantphos aryl signals and second [BArF$_4$]$^-$ peak), 1.66 (s, 6H, xantphos methyl signals), 1.84–0.50 (m, 33H, PCy$_3$). ^{31}P{^{1}H} NMR (202 MHz, CD$_2$Cl$_2$): δ 55.4 [dt, J(RhP) = 192, J(PP) = 34, PCy$_3$], 31.6 [dt, J(RhP) = 155, J(PP) = 34 Hz, xantphos]. ESI-MS (1,2-F$_2$C$_6$H$_4$, 60 °C, 4.5 kV): m/z 961.33 [M]$^+$ (calc. 961.33). Peak displays the expected isotopic pattern.

Acknowledgements

This journal is © The Royal Society of Chemistry 2014

Catal. Sci. Technol., 2014, 4, 3486–3494 | 3493

Notes and references

1 D. Mannig and H. Noth, *Angew. Chem., Int. Ed. Engl.*, 1985, **24**, 878–879.

2 J. Hartwig, *Organotransition metal chemistry: from bonding to catalysis*, University Science Books, Sausalito, 2010.

3 C. M. Crudden and D. R. Edwards, *Eur. J. Org. Chem.*, 2003, **2003**, 4695–4712.

4 T. Davan, E. W. Corcoran and L. G. Sneddon, *Organometallics*, 1983, **2**, 1693–1694.

5 K. Burgess, W. A. Van der donk, S. A. Westcott, T. B. Marder, R. T. Baker and J. C. Calabrese, *J. Am. Chem. Soc.*, 1992, **114**, 9350–9359.

6 D. A. Evans, G. C. Fu and B. A. Anderson, *J. Am. Chem. Soc.*, 1992, **114**, 6679–6685.

7 D. R. Edwards, Y. B. Hleba, C. J. Lata, L. A. Calhoun and C. M. Crudden, *Angew. Chem., Int. Ed.*, 2007, **46**, 7799–7802.

8 J. M. Brown and G. C. Lloyd Jones, *J. Am. Chem. Soc.*, 1994, **116**, 866–878.

9 A. Staubitz, A. P. M. Robertson, M. E. Sloan and I. Manners, *Chem. Rev.*, 2010, **110**, 4023–4078.

10 M. Scheideman, G. Wang and E. Vedejs, *J. Am. Chem. Soc.*, 2008, **130**, 8669–8676.

11 E. M. Leitao, T. Jurca and I. Manners, *Nat. Chem.*, 2013, **5**, 817–829.

12 L. J. Sewell, M. A. Huertos, M. E. Dickinson, A. S. Weller and G. C. Lloyd-Jones, *Inorg. Chem.*, 2013, **52**, 4509–4516.

13 L. J. Sewell, G. C. Lloyd-Jones and A. S. Weller, *J. Am. Chem. Soc.*, 2012, **134**, 3598–3610.

14 L. J. Sewell, A. B. Chaplin and A. S. Weller, *Dalton Trans.*, 2011, **40**, 7499–7501.

15 In this report we did not describe H/D labelling studies. Subsequent studies using $D_3B \cdot NMe_3$ showed that alkene coordination and deuteride insertion to form the linear product where all reversible, as found in this current study and consistent with reductive elimination being the rate-determining step at the early stages of catalysis. L. J. Sewell, *DPhil Thesis*, University of Oxford, 2013.

16 M. Toure, O. Chuzel and J.-L. Parrain, *J. Am. Chem. Soc.*, 2012, **134**, 17892–17895.

17 M. Kranenburg, Y. E. M. van der Burgt, P. C. J. Kamer, P. W. N. M. van Leeuwen, K. Goubitz and J. Fraanje, *Organometallics*, 1995, **14**, 3081–3089.

18 H. C. Johnson, C. L. McMullin, S. D. Pike, S. A. Macgregor and A. S. Weller, *Angew. Chem., Int. Ed.*, 2013, **52**, 9776–9780.

19 T. M. Douglas, A. B. Chaplin, A. S. Weller, X. Yang and M. B. Hall, *J. Am. Chem. Soc.*, 2009, **131**, 15440–15456.

20 G. Alcaraz and S. Sabo-Etienne, *Coord. Chem. Rev.*, 2008, **252**, 2395–2409.

21 A. B. Chaplin and A. S. Weller, *Inorg. Chem.*, 2010, **49**, 1111–1121.

22 W. H. Bernskoetter, C. K. Schauer, K. I. Goldberg and M. Brookhart, *Science*, 2009, **326**, 553–556.

23 M. D. Walter, P. S. White, C. K. Schauer and M. Brookhart, *J. Am. Chem. Soc.*, 2013, **135**, 15933–15947.

24 S. D. Pike, A. L. Thompson, A. G. Algarra, D. C. Apperley, S. A. Macgregor and A. S. Weller, *Science*, 2012, **337**, 1648–1651.

25 Y. Kawano, K. Yamaguchi, S. Y. Miyake, T. Kakizawa and M. Shimoi, *Chem. – Eur. J.*, 2007, **13**, 6920–6931.

26 Related $Rh(PR_3)_2(\eta^2\text{-carborane})$ complexes have been reported as the resting states during cage B-H hydroboration reactions with alkenes: J. D. Hewes, C. W. Kreimendahl, T. B. Marder and M. F. Hawthorne, *J. Am. Chem. Soc.*, 1984, **106**, 5757–5759; E. Molinos, S. K. Brayshaw, G. Kociok-Köhn and A. S. Weller, *Organometallics*, 2007, **26**, 2370–2382.

27 R. B. Jordan, *Reaction Mechanisms of Inorganic and Organometallic Systems*, Oxford University Press, 2007.

28 A. T. Lubben, J. S. McIndoe and A. S. Weller, *Organometallics*, 2008, **27**, 3303–3306.

29 K. L. Vikse, M. P. Woods and J. S. McIndoe, *Organometallics*, 2010, **29**, 6615–6618.

30 L. P. E. Yunker, R. L. Stoddard and J. S. McIndoe, *J. Mass Spectrom.*, 2014, **49**, 1–8.

31 A. B. Chaplin and A. S. Weller, *Angew. Chem., Int. Ed.*, 2010, **49**, 581–584.

32 A. G. Algarra, L. J. Sewell, H. C. Johnson, S. A. Macgregor and A. S. Weller, *Dalton Trans.*, 2014, DOI: 10.1039/c3dt52771a.

33 Reliable integration to quantify the degree of H/D exchange in the borane was frustrated by the quadrupolar-broadened signals.

34 R. T. Baker, J. C. Calabrese, S. A. Westcott, P. Nguyen and T. B. Marder, *J. Am. Chem. Soc.*, 1993, **115**, 4367–4368.

35 D. E. Kadlecek, P. J. Carroll and L. G. Sneddon, *J. Am. Chem. Soc.*, 2000, **122**, 10868–10877.

36 E. Molinos, S. K. Brayshaw, G. Kociok-Köhn and A. S. Weller, *Organometallics*, 2007, **26**, 2370–2382.

37 T. C. Morrill, C. A. D'Souza, L. Yang and A. J. Sampognaro, *J. Org. Chem.*, 2002, **67**, 2481–2484.

38 E. M. Simmons and J. F. Hartwig, *Angew. Chem., Int. Ed.*, 2012, **51**, 3066–3072.

39 R. Ghosh, T. J. Emge, K. Krogh-Jespersen and A. S. Goldman, *J. Am. Chem. Soc.*, 2008, **130**, 11317–11327.

40 A. E. W. Ledger, C. E. Ellul, M. F. Mahon, J. M. J. Williams and M. K. Whittlesey, *Chem. – Eur. J.*, 2011, **17**, 8704–8713.

41 M. A. Huertos and A. S. Weller, *Chem. Sci.*, 2013, **4**, 1881.

42 M. A. Huertos and A. S. Weller, *Chem. Commun.*, 2012, **48**, 7185–7187.

43 T. N. Hooper, M. A. Huertos, T. Jurca, S. D. Pike, A. S. Weller and I. Manners, *Inorg. Chem.*, 2014, **53**, 3716–3729.

44 R. Dallanegra, A. B. Chaplin and A. S. Weller, *Organometallics*, 2012, **31**, 2720–2728.

45 A. J. Sandee, L. A. van der Veen, J. Reek, P. Kamer, M. Lutz, A. L. Spek and P. van Leeuwen, *Angew. Chem., Int. Ed.*, 1999, **38**, 3231–3235.

46 R. J. Pawley, G. L. Moxham, R. Dallanegra, A. B. Chaplin, S. K. Brayshaw, A. S. Weller and M. C. Willis, *Organometallics*, 2010, **29**, 1717–1728.

3494 | *Catal. Sci. Technol.*, 2014, **4**, 3486–3494

This journal is © The Royal Society of Chemistry 2014